

See discussions, stats, and author profiles for this publication at: <https://www.researchgate.net/publication/225605878>

Nanoparticle Geometrical Effect on Structure, Dynamics and Anisotropic Viscosity of Polyethylene Nanocomposites

ARTICLE *in* MACROMOLECULES · FEBRUARY 2012

Impact Factor: 5.8 · DOI: 10.1021/ma202289a

CITATIONS

31

READS

71

3 AUTHORS, INCLUDING:



Martin Kröger

ETH Zurich

239 PUBLICATIONS 3,828 CITATIONS

[SEE PROFILE](#)

Nanoparticle Geometrical Effect on Structure, Dynamics and Anisotropic Viscosity of Polyethylene Nanocomposites

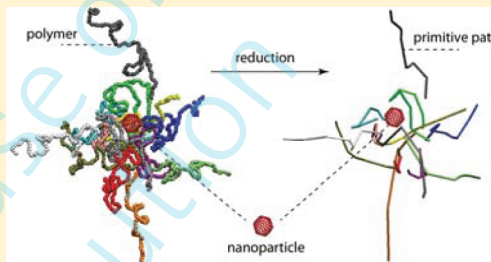
Ying Li,[†] Martin Kröger,[‡] and Wing Kam Liu^{*,†,§}

[†]Department of Mechanical Engineering, Northwestern University, 2145 Sheridan Road, Evanston, Illinois 60208-0311, United States

[‡]Department of Materials, Polymer Physics, ETH Zurich, CH-8093 Zurich, Switzerland

[§]Visiting Distinguished Chair Professor, School of Mechanical Engineering, World Class University (WCU) Program in Sungkyunkwan University, Korea

ABSTRACT: Addition of nanoparticles into a polymer matrix can significantly alter its structure, dynamics as well as viscosity. In this paper, we study the structural, dynamical and viscous behaviors of polyethylene (PE) matrices under the influence of five differently shaped nanoparticles: buckyball, graphene, nanodiamond (ND), X-shaped and Y-shaped junctions, at fixed volume fraction (4 vol %). These nanoparticles have different surface-area-to-volume ratios, arranged as graphene, X-shaped junction, Y-shaped junction, buckyball, and ND, from the largest to the smallest. In turn, different interaction energies between nanoparticles and PE matrices are enabled according to their surface-area-to-volume ratios. The graphene sheet is expected to have the strongest interaction with the PE matrix in accord with its largest surface-area-to-volume ratio. The interaction between NDs and their PE matrix is the smallest, due to their truncated octahedron shapes and the smallest surface-area-to-volume ratio. However, the graphene sheets tend to aggregate at the PE melting temperature (450 K), lowering their interactions with the PE matrix. Because of this interplay, the interactions between nanoparticles and polymer matrices can be tailored through the shapes (also surface-area-to-volume ratios) of nanoparticles as well as their dispersions. The polymer chains are found to be densely packed around these nanoparticles in the range of 2 nm, except NDs, due to their strong interactions with PE matrices. Thus, these nanoparticles are found to be able to nucleate polymer entanglements around their surfaces and to increase the underlying entanglement densities of PE matrices. Both the polymer chain relaxation and anisotropic viscosity of PE nanocomposites are shown to be greatly affected by oriented nanoparticles. Our simulation results indicate that the surface-area-to-volume ratio of nanoparticles plays the dominated role in the structural, dynamical and viscous properties of PE nanocomposites.



1. INTRODUCTION

The viscoelastic properties of polymers originate from their chain dynamics. For low molecular weight polymers, the viscosity is mainly induced by the monomer–monomer friction between different polymer chains (Rouse relaxation).¹ However, above the entanglement molecular weight M_e , the different polymer chains can mutually interpenetrate each other and self-entangle, driven by entropy. Since polymer chains cannot cross each other as they move, the dynamics of polymer chains is constrained (chain connectivity and uncrossability). Entanglements are commonly assumed to severely restrict the lateral motion of individual polymer chains into a tube-like region. The lateral motion of individual polymer chains is confined to the length scale of the tube diameter. Therefore, a polymer chain tends to move only back and forth, i.e. reptate, along the central axis of the tube, also denoted as primitive path (PP). The PP is considered as the shortest path remaining when one holds chain ends fixed, while continuously reducing (shrinking) a chain's contour without violating topological constraints (entanglements). Relaxation of a polymer chain is achieved by completely diffusing out of its original tube and forming another new tube. Such a conceptual

framework, the tube model, developed by de Gennes² and later generalized by Doi and Edwards,³ has incorporated such a principle for studying the dynamics of polymer chains. The viscoelastic properties of polymers are described by the tube model within a mean-field approach³ as the reptation is considered as a one-dimensional diffusion along the PP. Although the tube model can be used to capture the essential part of the entanglements dynamics, there are two refinements which have been incorporated to deal with PP contour length fluctuations (CLF)^{4,5} and many-body effects. The latter, known as constraint release (CR),^{4,6} considers the lateral softening of the confined tube, as both the chain and its virtual tube are equally moving under melt.

Fillers with dimensions on the micrometer scale are added into polymers in conventional polymer composites, as to enhance their mechanical properties. Such properties are highly related to volume fraction, shape and size of these fillers. If the size of fillers is on the nanometer scale, their mixtures with a

Received: October 12, 2011

Revised: January 23, 2012

Published: February 7, 2012

polymer matrix lead to so-called *polymer nanocomposites* (PNC). Compared to traditional polymer composites, the physical and mechanical properties of PNC can be remarkably enhanced by the addition of only a small volume fraction of nanoparticles. Therefore, PNC has attracted much interest both in industry and academia. The enhancement of mechanical performance of PNC, is mainly due to the nanoscale of fillers (because of extremely high surface-area-to-volume ratio), and to the strong polymer–nanoparticle interactions that can affect the loading transfer effectiveness between nanoparticles and polymer matrix. Since the motion of polymer chains is mainly constrained by entanglements for pure polymers, it is not hard to see that additional geometrical constraints are added into the pure polymers when the nanoparticles are infused. Therefore, the underlying PP network of polymers may also be affected by the presence of nanoparticles.

Several decades ago, Bueche assumed that entanglements nucleate at the surface of fillers, and effectively modify the underlying PP network of the polymer matrix.⁷ Thus, the amount of surface area plays the major role in the reinforcement effect of nanoparticles.⁷ More recently, Schneider et al⁸ studied the dynamics of entangled polymer chains in PNC by neutron spin echo (NSE) experiments. They found that the basic Rouse relaxation rate was unaffected by the high volume fraction of nanoparticles.⁸ However, the lateral confinement of polymer chains or tube diameter decreased with the increment of nanoparticle concentration, as a crossover from “polymer entanglements” to “nanoparticle entanglements” (chain motion is hindered by the fixed obstacles) occurs due to the geometrical confinement effect of these nanoparticles.⁸ Our focus in this paper is then to investigate the microscopic origin of the observed behavior, as we study microscopic details such as entanglements, and orientations of polymer chains around nanoparticles, etc.

In recent years, computer simulations have successfully captured the PP network of polymers.^{9–19} These simulation methods have been widely used for analyzing the PPs of polymer melts under both static and shear flow conditions.^{9,10,12,13,17,20} The obtained results are useful for predicting and understanding viscoelastic properties of pure polymers.²¹ Using these approaches, de Pablo and co-workers have done the pioneering works to study the PP network of entangled polymer matrix influenced by the spherical or rod-like nanoparticles.^{20,22} They found that nanoparticles had significant impact on the entanglement network of the polymer matrix, served as entanglement attractors, especially at large deformations, which shed light on how the nanoparticles influence the viscoelastic properties of PNCs.²² However, due to the limitation of computer power, many simulations have been limited to PNC with polymer chain lengths well below the entanglement molecular weight.^{23–25} For the study of high molecular weight polymers, Monte Carlo (MC) methods are usually invoked, but they do not supply information about polymer chain dynamics. To overcome these shortcomings, we used the latest processor generation and performed long-time molecular dynamics (MD) simulations on polyethylene (PE) nanocomposites under the melt conditions. There are several aspects where this paper differs from past works. First, we simulate truly entangled PE nanocomposites at equilibrated conditions with differently shaped nanoparticles. The size of these nanoparticles is comparable with the size of polymer chains, which has great impact on the motion of PE polymer chains. Second, the effect of differently shaped nanoparticles on

the structure and dynamical relaxation of PE matrix will be considered, which is directly related to the nanoparticle–polymer interactions. The dispersion/clustering effect of nanoparticles is also considered in this work. Third, the underlying PP networks of PE matrices with different nanoparticles are extracted by modified Z1 code,¹⁵ as well as the underlying entanglement distributions, which can help us to understand how the viscoelastic properties of PNC will be affected by different nanoparticles. In short, we will study the effects of nanoparticle shape and their dispersion/clustering on the structure, dynamics, PP network and anisotropic viscosity of PE matrices, having in mind targeting a rational design of PNCs with optimal structural and mechanical properties.

2. MODEL AND METHODOLOGY

Carbon-based nanoparticles, i.e., single-walled carbon nanotubes (SWNTs), are well-known for their extremely high mechanical properties (Young's modulus is around 1–5TPa and tensile strength is 100–150 GPa).^{26,27} They have attracted much interest as reinforcing nanoparticles in PNC. In this paper, five different shapes of carbon components, i.e., buckyball, graphene, nanodiamond (ND), X-shaped SWNT junction and Y-shaped SWNT junction as shown in Figure 1,

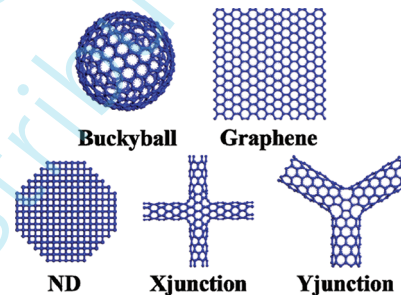


Figure 1. Models of buckyball, graphene, nanodiamond (ND), Xjunction and Yjunction used in PE nanocomposites. All these carbon nanoparticles have sp^2 bonds, except the ND (sp^3 bonds), which are indicated by the dots around covalent bonds. The shape of the ND is a truncated octahedron.

are used to generate different PE nanocomposites. The specifications of all these nanoparticles are summarized in Table 1. Here the graphene sheet was cut along armchair and

Table 1. Geometrical Details for Carbon Nanoparticles Used in This Work

	buckyball	graphene	ND	Xjunction	Yjunction
size (Å)	diameter 16.15	length 29	diameter 21.0	diameter 4.70	diameter 6.26
carbon atoms	320	width 29.8	length 14.66	length 14.66	length 14.82

zigzag directions, where length and width were along zigzag and armchair directions, respectively. The shape of ND is round-like, i.e., a truncated octahedron. A (6,0) SWNT with length 14.66 Å was utilized for the construction of the X-shaped SWNT junction. However, the Y-shaped SWNT junction was built from a (8,0) SWNT with length 14.82 Å. The details for constructing X-shaped and Y-shaped SWNT junctions can be found in refs 28–30. All the covalent bonds in these carbon



nanoparticles are sp^2 bonds, except for the ND, which has sp^3 bonds. Although the surface of ND can form some sp^2 bonds, we do not consider these sp^2 bonds and simplify them into sp^3 bonds in our simulations. The pure PE polymer and PE matrices were represented by united atom $-CH_2-$ units, which were connected to form a straight, linear PE polymer chain. In order to study entangled and high-molecular-weight polymers, we considered PE polymers with $N = 240$ monomers per chain in the current work with molecular weight $M_w = 3362$ g/mol. The entanglement length, N_e , defined as the ratio between the number of monomers and the mean number of entanglements per chain, is about 56–86 at 463 K, according to different experimental and simulations results.^{12,13,21} The PE polymer studied in the current work is truly entangled as $N/N_e = 2.79$ –4.28.

The molecular model for pure PE was generated with the Amorphous Cell Module in Materials Studio³¹ using the self-avoiding random walk technique.³² The initial molecular structures of PE nanocomposites were obtained through positioning the center of each nanoparticle coincident with the center of its cubic simulation box, while symmetric planes of the nanoparticle were parallel to the facets of the simulation box. Then, PE polymer chains were randomly generated around nanoparticles and used for filling the simulation box based on the self-avoiding random walk technique.³² These nanoparticles were added into PE matrices at approximately 4 vol %. After initial configurations were generated, all these models were repeated once along x, y and z directions of the simulation box to obtain the initial systems with large enough samples (polymer chains). Therefore, each PE nanocomposite has 8 nanoparticles, which are initially arranged into a cubic crystal-like structure. The number of polymer chains and geometry size for the initial pure PE and PE nanocomposite models are listed in Table 2. In order to simplify notations, the

Table 2. Initial Simulation Box Size at Melt Temperature (450 K) and Polymer Chain Numbers of Pure PE Polymer and Its Nanocomposites^a

	PE	PE/ Bucky	PE/ Graphene	PE/ ND	PE/ Xjunction	PE/ Yjunction
side length (Å)	97.0	95.4	84.2	104.6	87.3	95.3
polymer chain number	112	104	72	136	80	104

^aThe volume fractions of nanoparticles are fixed to be 4 vol %.

terms PE/Bucky, PE/Graphene, PE/ND, PE/Xjunction and PE/Yjunction are used for PE/buckyball, PE/graphene, PE/ND, PE/X-shaped junction and PE/Y-shaped junction nanocomposites, respectively. The pure PE polymer is also abbreviated as PE. Once the initial molecular structures are obtained, the corresponding force field should be assigned for future MD simulations. The PE polymer chain was described by appropriate bond, angle and dihedral, as well as nonbonded van der Waals (vdW) interactions. The united-atom representation for PE is adopted in this work as carbon atoms along with their bonded hydrogen atoms are lumped into single interacting sites. The methylene (CH_2) and methyl (CH_3) groups are treated as equivalent sites for all bonded interactions, but, not for vdW interactions. Such a united-atom model has been widely used and verified for studying diffusion

and melting behaviors of PE polymers.^{9,13,17,18,33–38} In order to explore the nanoparticle shape effect on PE matrices, all these carbon nanoparticles were modeled as nondeformable rigid bodies.³⁹ The bond length for these nanoparticles with sp^2 and sp^3 bonds was fixed to be 1.42 and 1.54 Å, respectively. The interactions between different nanoparticles are also modeled by vdW potentials. The potential forms with corresponding parameters are summarized in Table 3. The vdW interactions

Table 3. Functional Forms and Parameters for the Force Fields of PE and Carbon Nanoparticles Used in This Paper

interaction type (potential type)	functional form	parameters
bond (harmonic)	$U(r) = k_r(r - r_0)^2$	$k_r = 419.518$ kcal/mol/Å ² , $r_0 = 1.54$ Å
angle (harmonic)	$U(\theta) = k_\theta(\theta - \theta_0)^2$	$k_\theta = 62.09$ kcal/mol/deg ² , $\theta_0 = 114^\circ$
dihedral (multiharmonic)	$U(\phi) = \sum_{i=0,3} a_i \cos^i(\phi)$	$a_0 = 1.736$ kcal/mol, $a_1 = 4.500$ kcal/mol $a_2 = 0.764$ kcal/mol, $a_3 = -7.000$ kcal/mol
nonbonded (Lennard-Jones)	$U(r) = 4\epsilon[(\sigma/r)^{12} - (\sigma/r)^6]$	$\epsilon_{CH_3} = 0.227$ kcal/mol, $\sigma_{CH_3} = 4.01$ Å $\epsilon_{CH_2} = 0.093$ kcal/mol, $\sigma_{CH_2} = 4.01$ Å $\epsilon_C = 0.105$ kcal/mol, $\sigma_C = 3.367$ Å

between PE monomers and carbon atoms of nanoparticles were obtained through the Lorentz–Berthelot rules of the 12–6 Lennard-Jones potentials between their vdW potential parameters. All the MD simulations were performed using the LAMMPS package supplied by Sandia National Laboratory.⁴⁰ Periodic boundary conditions were used as the simulation box was considered to be a representative volume element (RVE). The time step for MD simulations was 1.0 fs. All the simulations have been done at 450 K.

3. SELF-ASSEMBLY BEHAVIOR OF NANOPARTICLES

As the initial arrangement of the carbon nanoparticles is cubic crystal-like, we have carried out long MD simulations for all these PE nanocomposites to reach their equilibrium states. The simulations have been done under the NPT ensemble ($p = 1$ atm and $T = 450$ K) at a time step 1 fs for a duration of 200 ns. The shapes of nanoparticles are fixed through “rigid body” constraints.³⁹ The pair distribution functions $g(r)$ between different nanoparticles and their interaction energies have been monitored during the relaxation process. Interestingly, we find that nanoparticles tend to self-assemble, $g(r)$ systematically increases with time at short distances within the first 100 ns (Figures 2a–e). Accordingly, the interaction energies between nanoparticles increase with time and finally reach a constant value (Figure 2f). After 100 ns, the aggregated nanoparticle structure has been established. Figure 3 shows the equilibrated structures of pure PE and PE nanocomposites. We clearly see that all the nanoparticles in PE nanocomposites are clustered together. Starr et al. have studied the underlying clustering mechanisms of nanoparticles inside nanocomposites and obtained corresponding phase diagrams.²³ They found that the crossover from the dispersed to the clustered state of nanoparticles is in good agreement with predictions from equilibrium particles association or equilibrium polymerization, but, not the first-order phase separation model.²³ The critical volume fraction φ for nanoparticle self-aggregation is related to

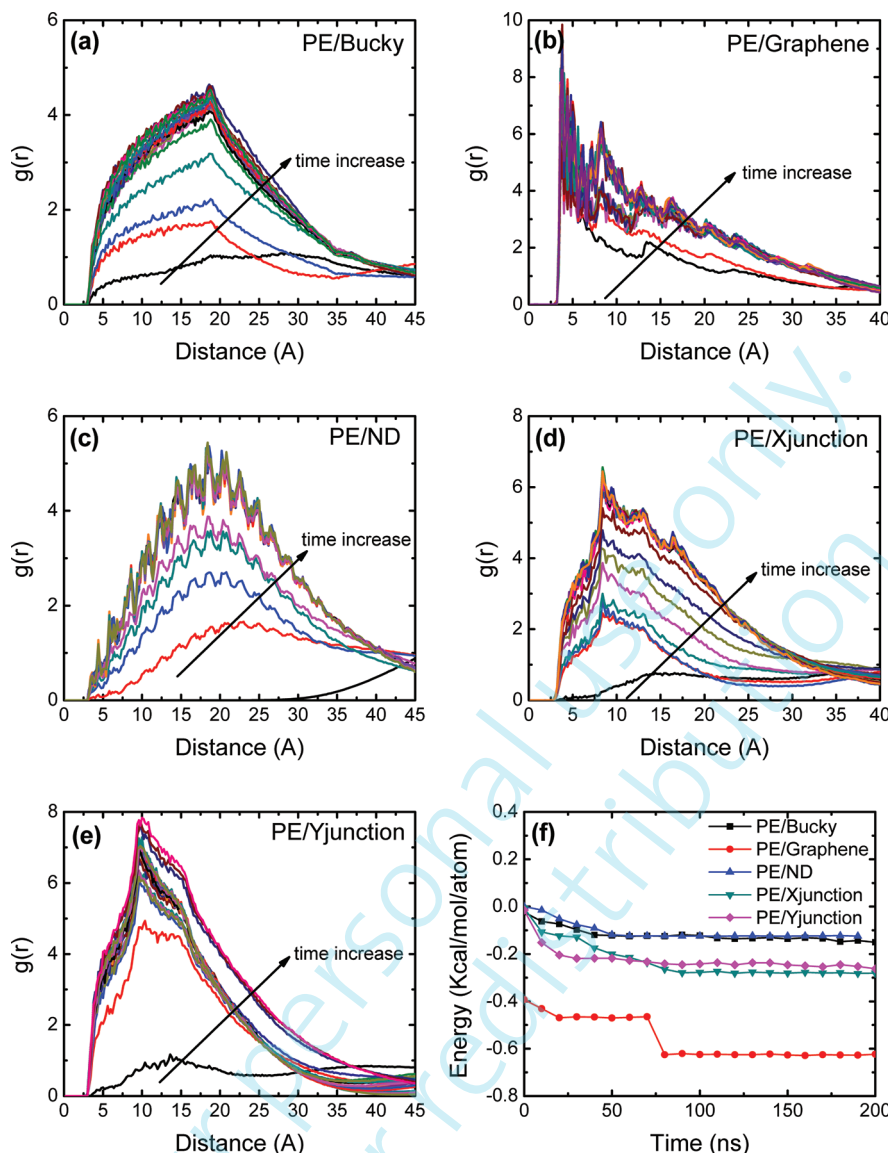


Figure 2. Evolution of pair distributions $g(r)$ between nanoparticles during the relaxation process for (a) PE/Bucky, (b) PE/Graphene, (c) PE/ND, (d) PE/Xjunction, and (e) PE/Yjunction at 450 K. The interaction energy between different nanoparticles is shown in part f.

the processing temperature as $\phi \sim \exp(-E_1^*/T^*)$, where E_1^* and T^* denote the thermal activation energy, $E_1^* = 6.9$, and system temperature in reduced LJ units, respectively.²³ As we know, the reduced temperature $T^* = 1$ corresponds to $T = 443$ K for pure PE.⁴¹ Therefore, the critical volume fraction for nanoparticle clustering is only about 0.1 vol % in PE nanocomposites at 443 K, a value small compared to the 4 vol % employed here. To study well dispersed nanoparticles at 4 vol % in PE nanocomposites, the processing temperature should be set to 207 K. This is one of the reasons why the solid-state shear pulverization (SSSP) process can produce the well dispersed particles in PNCs as the processing is always under low temperature.⁴²

As the nanoparticles tend to cluster, we consider two situations to explore the nanoparticle dispersion/clustering effect. One is an artificial, uniform nanoparticle distribution, denoted by 'U' (cubic crystal-like arrangement) as given in the initial conditions. The other is the fully equilibrated, more random distribution so-called 'R' as shown in Figure 3. The PE nanocomposites with uniformly dispersed nanoparticles are also

equilibrated under the NPT ensemble ($p = 1$ atm and $T = 450$ K) for 100 ns, while all the motions of nanoparticles are frozen in this process to keep their arrangement fixed. The vdW surfaces and volumes of the 8 nanoparticles under both situations are listed in Table 4. The vdW radius of each carbon atom of a nanoparticle is considered as 3.4 Å (Table 3). These nanoparticles can be arranged as graphene, Xjunction, Yjunction, buckyball, and ND, according to their aspect ratios from the largest to the smallest. Such an order will be directly related to the structural, dynamical and viscous properties of PE nanocomposites, which we will discuss later. We can also see that both the vdW surfaces and volumes of the carbon nanoparticles reduce after the clustering, and that this effect is especially pronounced for graphene. Prior to self-aggregation, the graphene nanoparticles have the largest surface over volume aspect ratio as 0.731 \AA^{-1} . This value drops to 0.551 \AA^{-1} after the clustering occurred. This phenomenon is directly related to the interactions between nanoparticles and PE matrices, which can help us to understand their viscous behaviors, to be discussed in the following parts.

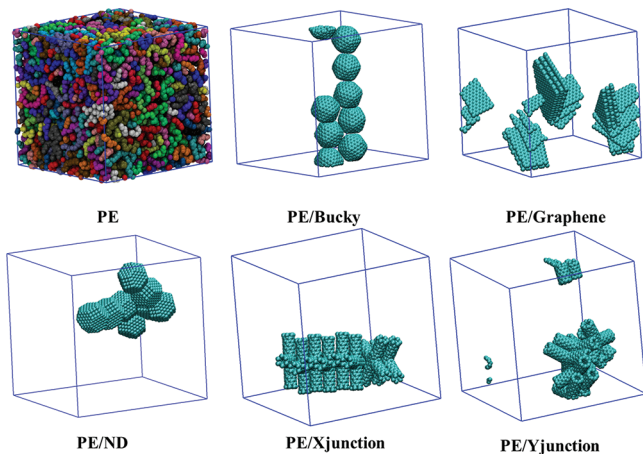


Figure 3. Equilibrated configurations for pure PE, PE/Bucky, PE/Graphene, PE/ND, PE/Xjunction, and PE/Yjunction at 450 K. All the nanoparticles are self-assembled together in the equilibration process. The simulation boxes are represented by blue lines. The different polymer chains are colored differently (randomly) in PE. In PE nanocomposites, all the polymer chains are made invisible for clarity of carbon nanoparticles. The volume fractions of all these carbon nanoparticles are fixed to be 4 vol %.

4. POLYMER CHAIN DYNAMICS

By using the well-equilibrated initial configurations of pure PE and PE nanocomposites (with both uniformly dispersed and clustered nanoparticles), all these models are further relaxed by NPT simulations ($p = 1$ atm and $T = 450$ K) for another 100 ns with time step 1.0 fs. In this process, all the motions of nanoparticles are frozen to keep their positions fixed. Both the end-to-end unit vector autocorrelation function $\langle \mathbf{u}(t) \cdot \mathbf{u}(0) \rangle$ and the mean-squared displacement (MSD) of PE polymer chains have been recorded to study the polymer chain dynamics. Figure 4 shows $\langle \mathbf{u}(t) \cdot \mathbf{u}(0) \rangle$ of PE chains exponentially decreasing with increasing time. For both uniformly dispersed and clustered nanoparticles, the dynamics of corresponding PE chains are slowed down in the presence of nanoparticles. We have fitted the $\langle \mathbf{u}(t) \cdot \mathbf{u}(0) \rangle$ curves with the function $\exp(-(t/\tau_e)^\beta)$, where τ_e and β represent two fitting parameters. Ideally, β equals unity for Rouse chains and τ_e is the corresponding relaxation time. As the molecular weight of PE chains in this work is well above the entanglement molecular weight M_e , the dynamics of PE chains will be further constrained by entanglements and $\beta < 1$. We can see that the larger the relaxation time τ_e is, or the smaller β is, the slower the polymer chain relaxation is. The obtained values for τ_e and β are given in Table 5. The relaxation time of PE nanocomposites is always larger than that of the pure PE. Therefore, the dynamics of the PE polymer chains is crucially affected by the carbon nanoparticles. From $\langle \mathbf{u}(t) \cdot \mathbf{u}(0) \rangle$ curves of uniformly dispersed

PE nanocomposites (Figure 4a), we can see that these can be classified into three categories. The first one is pure PE, which has the fastest relaxation. The second one contains PE/buckyball, PE/ND and PE/Yjunction. The third one includes PE/graphene and PE/Xjunction, which have the slowest relaxation. These visual observations are in good agreement with the estimated relaxation times τ_e shown in Table 5. As qualitatively expected from the theory of ellipsoids of revolution,⁴³ the relaxation time τ_e follows a similar trend as the surface-area-to-volume ratio shown in Table 4: the larger the surface-area-to-volume ratio, the longer the relaxation time. Compared with the uniformly dispersed nanoparticles, the equilibrated PE nanocomposites with clustered nanoparticles exhibit faster relaxation, a point to be discussed in the following part. The MSD curves of these pure PE and PE nanocomposites show a similar trend (results not shown).

There are two important factors influencing the dynamical behavior of polymer chains in PNCs: first, the geometrical constraints or “particle entanglements” imposed by these nanoparticles, mainly characterized by the interactions between polymer matrix and nanoparticles, and second, the underlying topological change of the polymer matrix, i.e., entanglement density. Obviously, it is hard to distinguish between the two factors as they tend to be correlated. In this work, we will investigate these two effects qualitatively by studying the interaction energy between nanoparticles and polymer matrix, and the entanglement distribution through a PP network analysis. The nanoparticle–monomer pair correlation function $g_{12}(r)$ is determined to characterize local packing density of polymer chains around the nanoparticles as well as their interactions (Figure 5). We recall that the atomistic motions of nanoparticles are frozen in the underlying MD simulations. The $g_{12}(r)$ curve for PE/Bucky is basically identical with the one presented earlier by Adnan.³⁴ We observe that $g_{12}(r)$ vanishes between 0 and 3.4 Å for all these PE nanocomposites, and hereafter gradually increases with radial distance. The depleted region reflects the vdW wall thickness, which is identical for all these PE nanocomposites.³⁴ The intensity of $g_{12}(r)$ for all nanocomposites reaches a first peak at ≈ 5.0 Å, except for PE/ND, which does not exhibit any peak at this radial distance. The relative distribution of PE monomers as indicated by $g_{12}(r)$ is affected by the shape of nanoparticles. Apparently, more PE monomers tend to aggregate around the PE/Graphene interface compared with the other nanocomposites. There is also a sharper second peak in $g_{12}(r)$ for these nanocomposites at a radial distance smaller than 1.5 nm, except for PE/Bucky and PE/ND, presumably due to the low geometric symmetry of these nanoparticles. The interaction energies between nanoparticles and PE matrices are listed in Table 5. It can be seen that PE/Graphene has the largest interaction energy, while, PE/ND has the smallest. From the largest to the smallest interaction energy, these PE nanocomposites can be arranged

Table 4. Van der Waals Surface, S_{vdW} , and Volume, V_{vdW} , for Carbon Nanoparticles before and after Self-Assembling^a

nanoparticles	S_{vdW}^U (Å ²)	V_{vdW}^U (Å ³)	S_{vdW}^U/V_{vdW}^U (Å ⁻¹)	S_{vdW}^R (Å ²)	V_{vdW}^R (Å ³)	S_{vdW}^R/V_{vdW}^R (Å ⁻¹)
PE/Bucky	9846	30 325	0.325	9301	29 144	0.319
PE/Graphene	18 355	25 093	0.731	12 859	23 350	0.551
PE/ND	14 448	45 588	0.317	12 821	45 608	0.281
PE/Xjunction	13 603	24 184	0.562	12 604	24 059	0.524
PE/Yjunction	12 356	25 028	0.494	11 466	25 173	0.455

^aThe superscripts “U” and “R” denote the uniformly dispersed and clustered nanoparticles, respectively.

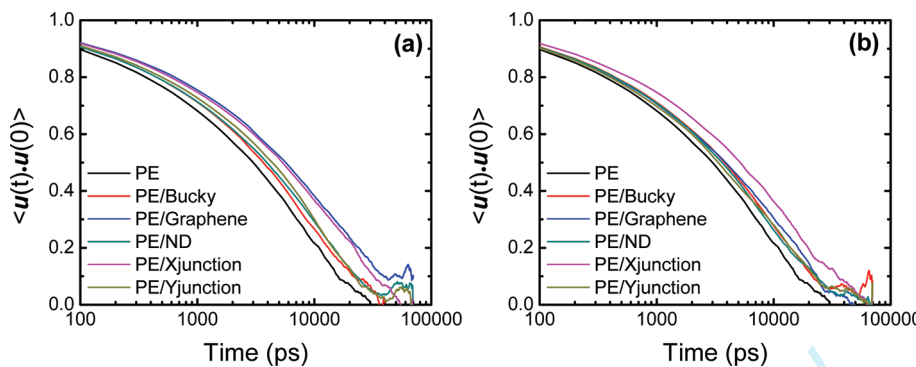


Figure 4. End-to-end unit vector autocorrelation function $\langle \mathbf{u}(t) \cdot \mathbf{u}(0) \rangle$ for PE polymer chains with (a) uniformly dispersed and (b) clustered nanoparticles at 450 K, respectively.

Table 5. Fitted Relaxation Time τ_e and Parameter β for End-to-End Unit Vector Autocorrelation Function $\langle \mathbf{u}(t) \cdot \mathbf{u}(0) \rangle = \exp(-(t/\tau_e)^\beta)$, Nanoparticle–Polymer Interaction Energy per Atom $E_{\text{PE,Carbon}}$, Root of the Mean-Squared End-to-End Distance $\langle R_{ee}^2 \rangle^{1/2}$ and Radius of Gyration $\langle R_g^2 \rangle^{1/2}$ for PE Polymer Chains as Well as Their Shear Viscosities (Shear Strain Rate $10^9/\text{s}$) at 450 K^a

	τ_e (ns)	β	$E_{\text{PE,Carbon}}$ (kcal/mol/atom)	$\langle R_{ee}^2 \rangle^{1/2}$ (Å)	$\langle R_g^2 \rangle^{1/2}$ (Å)	shear viscosity (cP)
PE	5.08	0.662	0	51.1 ± 1.7	20.7 ± 0.4	3.96 ± 0.45
PE/Bucky	6.30 (U)	0.633 (U)	-0.73 (U)	50.6 ± 1.8 (U)	20.2 ± 0.3 (U)	5.03 ± 0.63 (I)
	6.58 (R)	0.626 (R)	-0.60 (R)	53.4 ± 1.2 (R)	20.9 ± 0.4 (R)	5.10 ± 0.54 (O)
PE/Graphene	10.68 (U)	0.554 (U)	-1.14 (U)	50.2 ± 2.1 (U)	20.0 ± 0.3 (U)	3.21 ± 1.03 (I)
	7.19 (R)	0.571 (R)	-0.79 (R)	50.5 ± 3.0 (R)	20.5 ± 0.4 (R)	14.0 ± 3.17 (O)
PE/ND	6.89 (U)	0.615 (U)	-0.38 (U)	51.8 ± 1.4 (U)	21.8 ± 0.3 (U)	4.11 ± 0.47 (I)
	6.27 (R)	0.620 (R)	-0.31 (R)	53.2 ± 1.2 (R)	21.9 ± 0.2 (R)	4.50 ± 0.42 (O)
PE/Xjunction	9.91 (U)	0.562 (U)	-0.81 (U)	54.2 ± 2.5 (U)	21.2 ± 0.3 (U)	4.95 ± 0.82 (I)
	9.46 (R)	0.578 (R)	-0.58 (R)	52.2 ± 1.9 (R)	20.7 ± 0.5 (R)	8.98 ± 1.24 (O)
PE/Yjunction	7.25 (U)	0.652 (U)	-0.79 (U)	54.3 ± 1.3 (U)	21.1 ± 0.4 (U)	5.16 ± 0.68 (I)
	6.30 (R)	0.583 (R)	-0.55 (R)	51.9 ± 1.4 (R)	20.4 ± 0.3 (R)	6.52 ± 0.88 (O)

^a“U” and “R” represent the uniformly dispersed and clustered nanoparticle systems, respectively. “I” and “O” denote the in-plane and out-of-plane directions of the PE nanocomposites with uniformly dispersed nanoparticles.

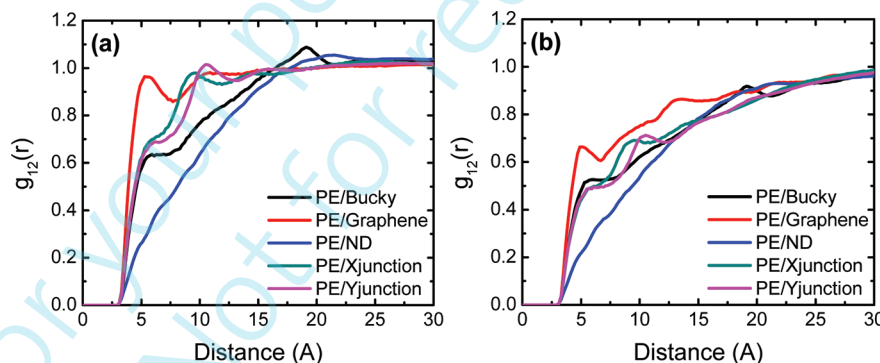


Figure 5. Nanoparticle–monomer pair distribution function $g_{12}(r)$ for PE nanocomposites with (a) uniformly dispersed and (b) clustered nanoparticles at 450 K.

as PE/Graphene, PE/Xjunction, PE/Yjunction, PE/Bucky, and PE/ND, which agrees reasonably well with their surface-area-to-volume ratios (Table 4). Such an order is also in good agreement with our $g_{12}(r)$ calculations (Figure 5a) and polymer chain relaxation (Figure 4a and Table 5). It is clearly shown that the stronger the nanoparticle–monomer interaction, the denser the packing of polymer chains around nanoparticles, and the slower polymer chains dynamics. When these nanoparticles are clustering together, the packing density of polymer chains around nanoparticles reduces (Figure 5b) as their vdW surface amount decreases (Table 4), leading to a reduction of the interaction energies between nanoparticles and PE matrices

(Table 5). For uniformly dispersed carbon nanoparticles, their interaction energy with the PE matrices is about 0.16–0.19 (kcal/mol)/Å². When these nanoparticles aggregate, this energy lowers further, down to 0.12–0.17 (kcal/mol)/Å². Recent experiments reported interaction energy between carbon black and styrene butadiene/silica rubber of only about 0.038 (kcal/mol)/Å².⁴⁴ Since carbon blacks are highly aggregated, it is important to make them well dispersed in the polymer matrices to improve their mechanical properties.

After the interaction energies between nanoparticles and PE matrices are known, it is interesting to explore how the global polymer chain conformation is affected by nanoparticles as a

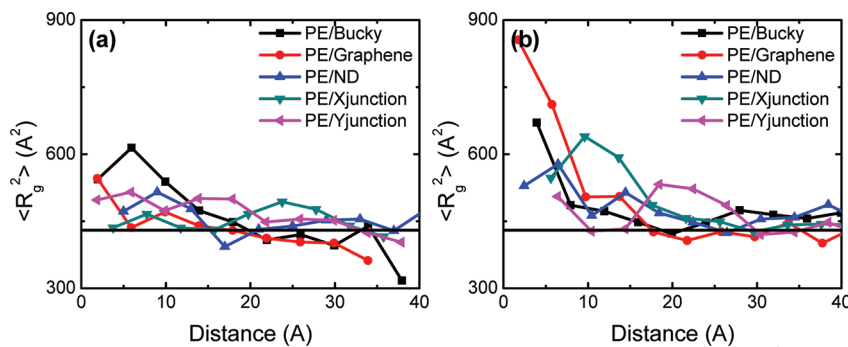


Figure 6. Mean-squared radius of gyration ($\langle R_g^2 \rangle$) of PE polymer chains at 450 K around (a) uniformly dispersed and (b) clustered nanoparticles as a function of their centers of mass from the center of the carbon nanoparticle. The horizontal line indicates the mean-squared radius of gyration of pure PE ($\sim 430 \text{ \AA}^2$) in the bulk.

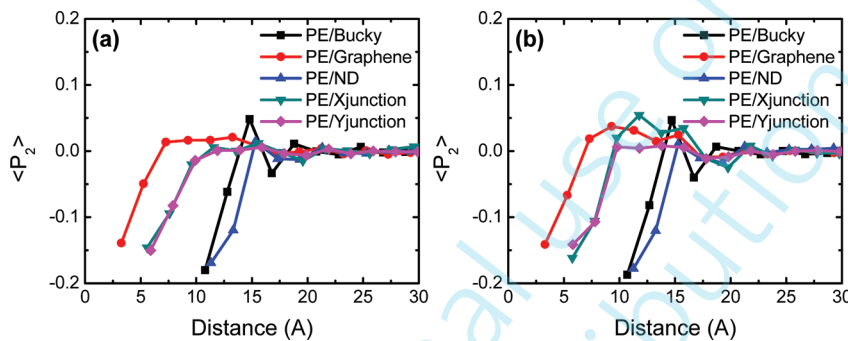


Figure 7. Mean second Legendre polynomial ($\langle P_2 \rangle$) between the vector from the center of the nanoparticle to the monomer i and the vector between i and the next monomer in the same PE polymer chain $i + 1$ with (a) uniformly dispersed and (b) clustered nanoparticles. The distance is from the centers of mass of these nanoparticles to the monomer i . A preferential alignment of the polymer chains parallel to the surface of the nanoparticle is observed.

function of the distance from the surface of nanoparticles to the centers of masses of the polymer chains. Since the surfaces of carbon nanoparticles studied by us are very irregular, except for buckyball and ND, we instead monitor the distance from the center of nanoparticles to the center of mass of each polymer chain. As we have 8 nanoparticles in each PE nanocomposite, the distance from the center of each nanoparticle to the center of mass of a single polymer chain is calculated first. The minimum value of these distances is the closest distance between a given polymer and a nanoparticle. The mean-squared radius of gyration ($\langle R_g^2 \rangle$) of this polymer is recorded at the same time. Figure 6 shows the ($\langle R_g^2 \rangle$) of polymer chains as a function of their distance from the center of the nearest nanoparticle for PE nanocomposites with both uniform and random dispersed nanoparticles. The conformation profiles of the PE polymer chains are slightly affected by the different shapes of nanoparticles. When the polymer chains are very close ($< 1 \text{ nm}$) to a nanoparticle in a system of well dispersed nanoparticles, they tend to be stretched as their ($\langle R_g^2 \rangle$) values are about 1.1–1.4 times of the ($\langle R_g^2 \rangle$) value of pure PE in its bulk state. Such a behavior is also observed by Starr et al.⁴⁵ and Ndoro et al.⁴⁶ The reference value 430 \AA^2 is obtained from the pure PE system. At distances larger than 2 nm, the ($\langle R_g^2 \rangle$) approaches the bulk behavior of PE. Therefore, if the interphase thickness is considered responsible for peculiarities concerning chain extension, it should be also in this range. After the nanoparticles are clustered together, the ($\langle R_g^2 \rangle$) profiles are greatly changed (Figure 6b). Polymer chains close to these clustered nanoparticles are highly stretched as the ($\langle R_g^2 \rangle$) value is about 1.2–2.0 times the bulk value. As the clustered

nanoparticles become very close to each other, they can be easily bridged by the polymer chains.⁴⁴ In this state, a polymer chain can be highly stretched and its ($\langle R_g^2 \rangle$) value is greatly increased. Such a bridging behavior is related to the nonlinear viscoelastic properties of PNCs, i.e., Payne effect.^{44,47} The averaged values of end-to-end distance ($\langle R_{ee}^2 \rangle^{1/2}$) and ($\langle R_g^2 \rangle^{1/2}$) for PE chains are listed in Table 5. ($\langle R_{ee}^2 \rangle \approx 6 \langle R_g^2 \rangle$) for pure PE indicates that it behaves as Gaussian coils. Interestingly, all the PE polymer chains have similar values of ($\langle R_{ee}^2 \rangle^{1/2}$) and ($\langle R_g^2 \rangle^{1/2}$).

Since the polymer chains are stretched near the surface of nanoparticles, their orientation might also be affected. To this end we calculate the second Legendre polynomial $P_2 = (3 \cos^2 \theta - 1)/2$, where θ is the angle formed between the vector connecting the center of the nanoparticle and monomer i , and the vector between i and the next monomer in the same PE polymer chain $i + 1$. The average orientation of the polymer chains is defined by taking the ensemble average ($\langle P_2 \rangle$). Here ($\langle P_2 \rangle = 0$) indicates a random orientation and ($\langle P_2 \rangle = -0.5$) for perfect tangential alignment.⁴⁸ Figure 7 shows the ($\langle P_2 \rangle$) as a function of distance from the center of mass of a polymer chain. When polymer chains are very close to the surface of nanoparticles, they are preferentially aligned tangentially to the surface of these nanoparticles as ($\langle P_2 \rangle = -0.2$ to -0.15). Moving away from the nanoparticle surface to the bulk polymer, ($\langle P_2 \rangle$) values gradually increase to zero, indicating they are randomly packed. Similar observations have been reported by Ndoro et al.⁴⁶ They found that the averaged orientational angle ($\langle \theta \rangle$) was around 85° ($\langle P_2 \rangle = -0.49$, if all angles are identical) when the polymer chains were near the spherical particle surfaces.⁴⁶ As the distance increases, ($\langle \theta \rangle$)

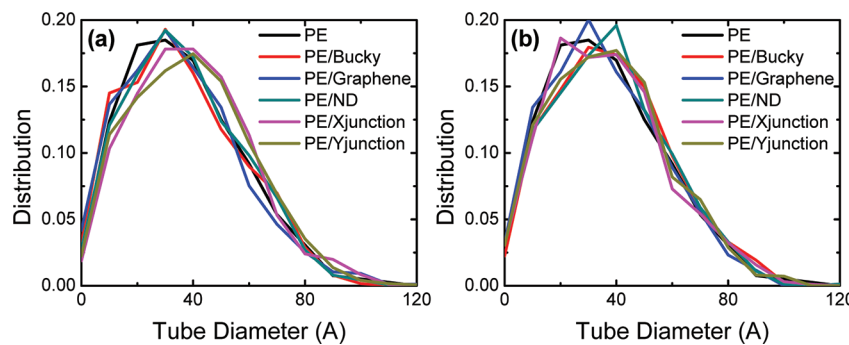


Figure 8. Distribution of tube diameter a_{pp} of pure PE and PE matrices with (a) uniformly dispersed and (b) clustered nanoparticles (see Appendix for details).

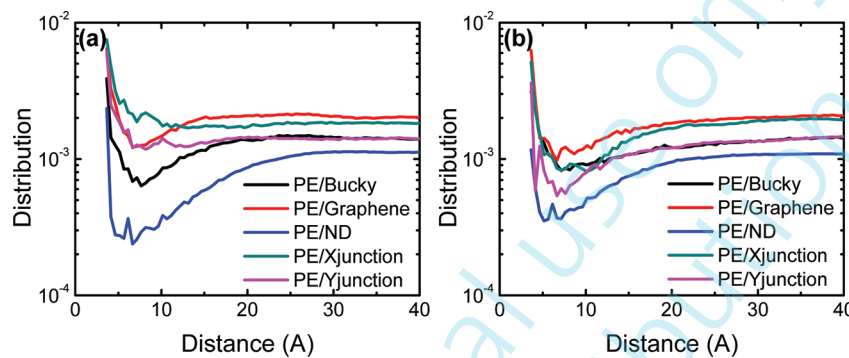


Figure 9. Nanoparticle-entanglement pair distributions of PE matrices with (a) uniformly dispersed and (b) clustered nanoparticles (see Appendix for details).

steadily decreases to approach its expected bulk value 57.3° ($\langle P_2 \rangle = -0.06$).⁴⁶ Obviously, the local orientational order only persists to a very short distance from the center of nanoparticles, i.e., 2 nm, small compared with the polymer chain extension measured by the root mean-square radius of gyration (Figure 6). Within view of Figure 6, the clustering effect of nanoparticles on the $\langle P_2 \rangle$ profiles is quite small as shown in Figure 7, and can even be ignored. In summary, the nanoparticles dispersion affects mainly the conformation of polymer chains, but not their orientations.

5. PRIMITIVE PATH ANALYSIS ON PE NANOCOMPOSITES

As the motion of polymer chains and their viscosity are known to be determined by their PP networks, the original Z1 code^{14,15} and its modified version, able to deal with nanoparticles, have been applied to pure PE polymer and PE nanocomposites to extract and study their PP networks (see Appendix for details). The obtained contour length of PP for pure PE is $\langle L_{pp} \rangle = 67.22 \pm 2.88$ Å, which agrees reasonably well with existing simulation results.¹² Also, from $\langle R_{ee}^2 \rangle$ and $\langle L_{pp} \rangle$, we can calculate the corresponding tube diameter of pure PE as $\langle a_{pp} \rangle = \langle R_{ee}^2 \rangle / \langle L_{pp} \rangle = 38.69$ Å, which is again in good agreement with both experimental ($\langle a_{pp} \rangle = 32.8$ Å with unknown M_w at 413 K⁴⁹) and simulation ($\langle a_{pp} \rangle = 37$ Å with $M_w = 3.36$ kg/mol at 450 K¹²) results. The average number of entanglements per chain $\langle Z \rangle$ for pure PE with $M_w = 3.36$ kg/mol studied in the current work is about 2.00 ± 0.11 . Therefore, we obtain an entanglement molecular weight $M_e = M_w / \langle Z \rangle = 1.68$ kg/mol, in agreement with both experimental and computational works ($M_e = 0.79\text{--}1.2$ kg/mol).²¹ Since the lateral motion of polymer chains is confined in the range of the

tube diameter a_{pp} , it is interesting to see the distribution of a_{pp} for each polymer chain under the influence of the nanoparticles. Figure 8 shows the distribution of a_{pp} for pure PE and PE nanocomposites with both uniformly dispersed and clustered nanoparticles. Interestingly, all these distributions follow the same trend, as the most favorable value for a_{pp} is about 10–60 Å (with probability >0.1). The distribution is well characterized by a beta function.¹² The peaks for the a_{pp} distributions of PE nanocomposites are slightly shifted to higher values, as well as their mean values ($\langle a_{pp} \rangle = 40\text{--}43$ Å). Such an observation also agrees reasonably well with recent experimental results.⁸ Schneider et al. found that the polymer chains in PNCs gradually disentangle as the volume fraction of nanoparticles increases, due to the transformation from “polymer entanglements” to “nanoparticles entanglements”.⁸ Therefore, the corresponding tube diameter $\langle a_{pp} \rangle$ of polymer matrices will also be gradually increased due to disentanglement, furthermore supported by mean-field theory.⁸ The predicted critical volume fraction is 35 vol %.⁸ When the volume fraction of nanoparticles is above 35 vol %, the polymer chain is expected to be completely disentangled and its motion is dominated by the geometrical constraints due to the nanoparticles.⁸ Similar to the distribution of tube diameter a_{pp} , the distributions of contour length of PP, L_{pp} , and the number of entanglements per chain, Z , for PE matrices are similar to that of pure PE polymer (Gaussian distributions, results not shown here). The dispersion/clustering effect of nanoparticles on the PP networks of PE matrices is negligible as shown in Figure 8. Since our nanoparticle concentration is only 4 vol %, we also do not expect to observe huge changes of the PP network of PE matrices, compared with pure PE. The PP network of PNCs

with highly loaded nanoparticles will be studied in our future work.

After the PP networks of PE matrices are extracted, we have access to the spatial distribution of entanglements. Figure 9 shows the pair distributions of nanoparticles to the entanglements of PE matrices. It is interesting to see that there are highly condensed entanglements near the nanoparticles surfaces, which is about 5–6 times of their bulk states. However, moving away from these nanoparticles surfaces to bulk polymer, the entanglement density rapidly drops, reaches a global minimum, and then gradually increases to a constant value. Because of the different nanoparticle shapes, the global minimum and bulk state—at a given concentration—of entanglement density are also changed. For the higher interaction energies, PE/Graphene and PE/Xjunction have larger bulk states of entanglement density than others. Also, PE/ND has the smallest global minimum and bulk state of entanglement densities, as the interaction between ND and PE matrix is very small (Table 5). Since polymer dynamics are constrained by entanglements as well as their densities, the geometrical confinement effect of nanoparticles on polymer chain entanglements is expected to affect the dynamics of these polymer chains. This picture is supported by the relaxation behavior of polymer chains in PE/Graphene and PE/Xjunction where it is significantly slowed down, compared to other PE nanocomposites and pure PE (Figure 4 and Table 5). Because of the dispersion/clustering effect, the bulk state of entanglement densities are also slightly decreased, as the interaction energies between nanoparticles and PE matrices are reduced (Table 5). The length scale for the variation of entanglement densities is around 2 nm, which is already present in the $\langle R_g^2 \rangle$ and $\langle P_2 \rangle$ profiles. Therefore, it is reasonable to suggest that the thickness of the interphase between carbon nanoparticles and PE matrices is around 2 nm.

By using the wall boundary model, Okuda et al. studied PP networks near the wall boundaries.⁵⁰ They made two assumptions: (1) polymer chains are not stuck, but randomly reflected by the wall boundaries and (2) the subchains below entanglement length behave like those in bulk state even though they are near the wall boundaries.⁵⁰ They found that the number of entanglements is increased near the wall boundaries due to the hooking process of their PP network models.⁵⁰ This finding is in good agreement with our current simulation results. However, we did not make any assumptions in our MD simulations and the PP networks are extracted based on our original PE matrices (real polymer chains). Papon et al. measured the local polymer chain dynamics near the surfaces of nanoparticles by low-field NMR.⁵¹ They found that at least three different kinds of polymer mobility existed in the filled elastomers, which are also in agreement with gradient T_g around the surfaces of nanoparticles (which cannot be described by a simple core–shell approximation).⁵¹ From our local entanglement distributions shown in Figure 9, we clearly see that the distribution profiles of entanglements are at least classified into three zones: high density (4–5 Å), low density (5–20 Å), and bulk density (20–40 Å), as the distance moving from the nanoparticle surfaces to the bulk polymer. Therefore, our PP network analysis as well as the distribution of entanglement density can be used to understand these local dynamical behaviors of polymer chains near nanoparticles surfaces from first principles.

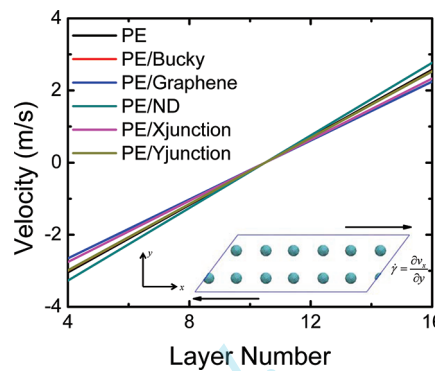


Figure 10. Velocity v_x profile in the simulation box along y direction for pure PE and PE nanocomposites with uniformly dispersed nanoparticles at 450 K, under the shear strain rate $10^9/\text{s}$. The simulation box is divided into 20 layers along y direction and only 4–16 layers are shown here (see Appendix for details). The layer thicknesses are 4.68 Å, 4.61 Å, 4.08 Å, 5.03 Å, 4.24 Å, and 4.60 Å, respectively, for PE, PE/Bucky, PE/Graphene, PE/ND, PE/Xjunction, and PE/Yjunction. The inset shows the simulation box of PE/Bucky under NEMD simulation. For clarity, the surrounding PE polymer chains are made invisible.

6. ANISOTROPIC VISCOSITY OF PE NANOCOMPOSITES

Employing the nonequilibrium molecular-dynamics (NEMD) method, we obtain the velocity v_x profile along the along y direction of the simulation boxes for pure PE polymer and PE nanocomposites with uniformly dispersed nanoparticles of fixed orientation, under a high shear strain rate $10^9/\text{s}$ (see Appendix for details). Obviously, the velocity gradient $\partial v_x / \partial y$ is uniform throughout all these systems, which indicates that these systems reached a steady-state shear flow. The shear viscosities of pure PE and PE nanocomposites with uniformly dispersed nanoparticles are obtained by $\eta = -\langle P_{xy} \rangle / \dot{\gamma}$, where $\langle P_{xy} \rangle$ is the time average over the xy -component of the pressure tensor and $\dot{\gamma}$ is the shear rate. The obtained value for pure PE ($M_w = 3.36 \text{ kg/mol}$) is $3.96 \pm 0.45 \text{ cP}$ at 450 K. Pearson et al. found that at low molecular weight, $M_w < M_c \approx 5 \text{ kg/mol}$, the zero-rate shear viscosity η_0 of PE is well described by the power law, $\eta_0 = 2.1 \times 10^{-5} M_w^{1.8}$ (cP) at 450 K.⁵² Obviously, our simulation result on pure PE is far away from the experimental result (46.78 cP), due to the shear thinning effect under high strain rate.⁹ Baig et al. have performed NEMD simulations on PE ($M_w = 5.60 \text{ kg/mol}$) over a broad range of different shear strain rates, under the melt condition ($T = 450 \text{ K}$).⁹ Under the strain rate $10^9/\text{s}$, the viscosity of PE ($M_w = 5.60 \text{ kg/mol}$) is estimated to be around 9 cP⁹, which is very well comparable with our simulation result ($3.96 \pm 0.45 \text{ cP}$ for $M_w = 3.36 \text{ kg/mol}$). The obtained viscosities of PE nanocomposites with uniformly dispersed nanoparticles are listed in Table 5. As the carbon nanoparticles considered in the current work have different symmetries, we calculate the viscosities of PE nanocomposites along in-plane (x) and out-of-plane (z) directions. It is interesting to see that the PE nanocomposites have different viscosities in different directions, especially for PE/Graphene and PE/Xjunction. For PE/Bucky, PE/ND, and PE/Yjunction, they have the similar viscosities both in x and z directions, due to their highly symmetrical structures. Also, the viscosities along the out-of-plane direction of PE nanocomposites are mainly determined by the interaction energy between nanoparticles and polymer matrix (or surface-area-to-volume ratio of

nanoparticles), which is in good agreement with our expectation.

The graphene and Xjunction nanoparticles are highly anisotropic. Therefore, the effective volumes occupied by these nanoparticles perpendicular to the flow direction are also anisotropic, especially for uniformly dispersed nanoparticles. To characterize the effective volume of a nanoparticle we use the gyration tensor, or moment of inertia tensor, $\mathbf{R} = n^{-1} \sum_{k=1}^n \mathbf{r}^k \mathbf{r}^k$ in its frame of principal axes, which corresponds to the orientation of the nanoparticles in their initial "U" states. Here \mathbf{r}^k is the position vector of the k th particle from the center of mass of the system to its atomistic position, and n is the total number of atoms in a nanoparticle. Therefore, we can calculate the gyration tensor \mathbf{R} for each single nanoparticle studied in the current work:

$$\mathbf{R} = \begin{bmatrix} 22.10 & 0 & 0 \\ 0 & 22.10 & 0 \\ 0 & 0 & 22.10 \end{bmatrix} (\text{\AA}^2) \text{ for buckyball}$$

$$\mathbf{R} = \begin{bmatrix} 73.85 & 0 & 0 \\ 0 & 72.46 & 0 \\ 0 & 0 & 0 \end{bmatrix} (\text{\AA}^2) \text{ for graphene}$$

$$\mathbf{R} = \begin{bmatrix} 22.10 & 0 & 0 \\ 0 & 22.10 & 0 \\ 0 & 0 & 22.10 \end{bmatrix} (\text{\AA}^2) \text{ for ND}$$

$$\mathbf{R} = \begin{bmatrix} 49.63 & 0 & 0 \\ 0 & 47.59 & 0 \\ 0 & 0 & 2.88 \end{bmatrix} (\text{\AA}^2) \text{ for Xjunction}$$

$$\mathbf{R} = \begin{bmatrix} 50.85 & 0.40 & -1.02 \\ 0.40 & 62.88 & -1.10 \\ -1.02 & -1.10 & 6.13 \end{bmatrix} (\text{\AA}^2) \text{ for Yjunction}$$

For the buckyball and ND, the principle diagonal elements of their gyration tensors are very close to each other, due to their spherical shapes. However, for the graphene sheet, due to its single-atom layer structure, its \mathbf{R} has a zero in its principle diagonal elements. From the wall boundary model study, the polymer chains perpendicular to the wall boundaries are greatly confined with increased entanglements, while the polymer chains parallel to these wall boundaries will be stretched and disentangled.⁵⁰ Therefore, for the PE/Graphene, the polymer chain dynamics will be accelerated by the graphene nanoparticles, when the shear flow is applied along its in-plane (x) direction. That is why we obtain a smaller viscosity value of PE/Graphene along its in-plane direction, compared with the bulk PE polymer. Because of the strong interactions between graphene nanoparticles and their PE matrix, the viscosity of PE/Graphene along its out-of-plane direction is almost four times that of pure PE. Similarly, the viscosity of PE/Xjunction along its out-of-plane direction is almost two times its viscosity along in-plane direction, due to the smaller diameter of its SWNT (also smaller R_{zz} value of its gyration tensor). However, for PE/Yjunction, this phenomenon is diminished, as the R_{zz} value of its gyration tensor is increased. From above discussions on interaction energies between nanoparticles and PE matrices as well as the PP analysis results, the PE/Graphene and PE/Xjunction with uniformly dispersed nanoparticles have larger

viscosities (along their out-of-plane directions), due to their stronger interaction energies and higher entanglement densities. Among all the PE nanocomposites with uniformly dispersed nanoparticles, PE/ND has the smallest viscosity in the out-of-plane direction, since the interaction energy between ND nanoparticles and their PE matrix is the weakest.

Knauert et al. studied the nanoparticle shape effect on PNC rheology via NEMD simulation.⁵³ Icosahedron, rod, and sheet-shaped nanoparticles were considered with very short, unentangled polymer chains (10–40 monomers per chain). They found that there was a relatively weak enhancement of the viscosity of PNCs by using the sheet nanoparticles.⁵³ However, in their studies, the nanoparticles tend to cluster together, thus greatly reducing the interaction energy between nanoparticles and polymer matrix, cf. Table 5. Thus, the viscosity enhancement induced by sheet nanoparticles can also be greatly reduced by nanoparticle clustering. We observe a similar effect in our NEMD simulations on PE nanocomposites with randomly dispersed nanoparticles. The viscosity of PE/Graphene is only slightly larger than that of PE/Bucky and PE/ND, due to nanoparticle aggregation (results not shown). Grest et al. studied the shear rheology of nanoparticle suspensions with differently shaped nanoparticles, i.e., jacks, rods, plates, and spheres.^{54,55} They found that the viscosity of the suspension was greatly increased by using jacks (with the arm length to diameter aspect ratio 21), due to their highly aggregated structures and large effective volumes.^{54,55} However, the arm length to diameter aspect ratios of X junction and Y junction studied in current works are only 3.1 and 2.4, respectively. Thus, the interaction energy between nanoparticles and polymer matrix, as well as the gyration tensor \mathbf{R} of clustered nanoparticles in the laboratory frame can be greatly changed. That is the reason we see that both graphene and X junction have comparable enhancement effects on the viscosity of PE nanocomposites.

7. CONCLUSIONS

To understand how the nanoparticle shapes affect structural, dynamical and viscous properties of their polymer nanocomposites, we performed extensive MD simulations on PE nanocomposites with five different nanoparticles: buckyball, graphene, ND, Xjunction, and Yjunction. We have revealed several key issues by analyzing the MD trajectories.

First, the nanoparticles tend to aggregate together under the conditions employed in our study, in agreement with theoretical considerations. Under the melting temperature (450 K), all the carbon nanoparticles surrounded by PE polymer chains self-assemble during the first 100 ns and form stable clusters. Compared with uniformly dispersed nanoparticles (cubic crystal-like distribution), the vDW surfaces and volumes of the nanoparticles are reduced upon clustering. Especially for graphene sheets, whose ratio of vDW surface area to volume is reduced from 0.731 to 0.551 \AA^{-1} .

Second, the surface-area-to-volume ratio (shape) of nanoparticles greatly influences the interactions between nanoparticles and their polymer matrices, as well as the packing behaviors of their surrounding polymer chains. The nanoparticles considered in this paper can be arranged as graphene, Xjunction, Yjunction, buckyball, and ND, from the largest to the smallest of their surface-area-to-volume ratios. Both the interaction energy and polymer chain packing follow the same trend. Because of the strongest interactions between graphene sheets and their PE matrix, the PE polymer chains are highly

packed around graphene sheets at 5 Å (from the surface of graphene sheets to polymer chains). However, we do not find evidence for highly packed polymer chains around ND nanoparticles, in accord with their weak interactions with the PE matrix. During the clustering of nanoparticles, their interaction with the polymer matrices weaken as their vDW surfaces decrease. In turn, the polymer chain densities surrounding these nanoparticles are reduced. In short, the stronger the interaction between nanoparticles and the polymer matrix, the denser the polymer chains surround the nanoparticles. While this is expected, we have provided a detailed quantitative analysis.

Third, the relaxation behavior of polymer chains is also affected by the surface-area-to-volume ratio (shape) of the nanoparticle, as a result of both the interaction between nanoparticle and polymer chains, as well as the nanoparticle-induced topological changes of polymer chains surrounding the nanoparticles. The interaction between graphene sheets and their PE matrix is the strongest among all the nanoparticles considered in current work; correspondingly, the relaxation time of their PE chains is the longest. On the contrary, the relaxation time of PE chains in PE/ND is the shortest, since the ND nanoparticles have the weakest interactions with their PE matrix. Similar to the packing behaviors of polymer chains around nanoparticles, the relaxation of polymer chains is found to be accelerated after these nanoparticles clustered together, as the interactions between nanoparticles and their polymer matrices are weakened during this process. From the PP network analysis on the PE nanocomposites, the pair distributions between nanoparticles and entanglements of polymers are also available. A large entanglement density is found at the surfaces of the nanoparticles. Moving away from the nanoparticle surfaces to bulk, the entanglement density rapidly decreases, reaches its global minimum state at 6.4 Å (away from the nanoparticle surface), and gradually increases to its bulk state. The PE/Graphene and PE/Xjunction are found to have the largest bulk entanglement density, while PE/ND has the smallest. Therefore, the relaxation of polymer chains in PE/Graphene, PE/Xjunction, and PE/ND are the slowest and the fastest, respectively. However, the overall PP networks of PE matrices are very similar to that of pure PE, since the volume fraction of nanoparticles is very low (only 4 vol %) and these systems are still “polymer entanglements” dominated, as we discussed in detail.

Fourth, the polymer chains close to nanoparticles are highly stretched and they are preferentially aligned parallel to the surfaces of nanoparticles. From the profiles of radius of gyration ($\langle R_g^2 \rangle$) and the second Legendre polynomial ($\langle P_2 \rangle$), polymer chains close to nanoparticle surfaces (around 2 nm from the nanoparticle surfaces) are affected. From the pair distributions between nanoparticles and the polymers entanglements, the entanglement densities are greatly changed in the range of 2 nm from the nanoparticle surfaces. Therefore, the interphase thickness of PE polymers with carbon nanoparticles is determined to be in the same range.

Fifth, the anisotropic viscosities of PE nanocomposites are greatly affected by the surface-area-to-volume ratios (shapes) of nanoparticles and their moment of inertia tensors. From our NEMD simulations, both in-plane and out-of-plane viscosities of PE nanocomposites are obtained. Because of the highly anisotropic structures of graphene and X junction, their out-of-plane viscosities are much larger than their in-plane viscosities. From their gyration tensors, we find that their R_{zz} components

are very small, compared with other elements in the principle diagonal directions. Therefore, the shear flows along the out-of-plane directions of PE/Graphene and PE/Xjunction are also greatly constrained by their in-plane effective volumes and their strong nanoparticle–polymer interactions (large surface-area-to-volume ratios), which in turn increase their out-of-plane viscosities. Because of the weak interactions between buckyballs/NDs and PE matrices (small surface-area-to-volume ratios), PE/Bucky and PE/ND have comparable viscosities with pure PE polymer, which indicates that the polymer chains in PE/Bucky and PE/ND are not greatly constrained by these nanoparticles.

From our current study, the surface-area-to-volume ratio of nanoparticles plays an important role in the mechanical properties of PNCs. Both the static and dynamical properties of polymer matrices are strongly affected by the surface-area-to-volume ratios of nanoparticles (nanoparticle–polymer interactions). Since the surface-area-to-volume ratios of nanoparticles can be easily tailored through the shapes of nanoparticles or their dispersion/clustering, we expect some motivations for experimental works to be performed. It is important to stress that the nanoparticle–polymer interaction considered in this work is mainly of physical nature, i.e., vDW interaction. As the surfaces of carbon nanoparticles can be chemically modified and bonded to polymer chains (chemical bonding or hydrogen bonding), it will be important to explore how these interactions will affect the dynamical and viscous properties of PNCs.

APPENDIX

A. *PP Network Analysis on PE Nanocomposites.* The original Z1 code^{12–15,56} constructs the PP network of a polymeric system by fixing the ends of all polymer chains. Hereafter, each polymer chain is replaced by a sequence of infinitesimally thin, impenetrable and tensionless straight lines. The length of these

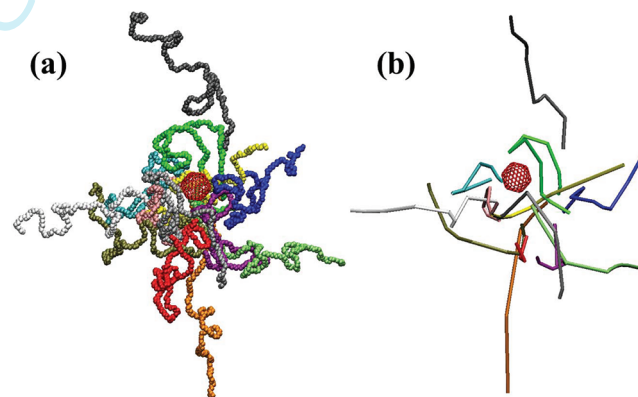


Figure 11. (a) Original molecular model of PE nanocomposites with a single buckyball and (b) its corresponding PP network under “frozen particle limit”. In part a, the different colored particles represent different polymer chains. In part b, the PPs are different colored straight lines and the buckyball is fixed in the space in the topological analysis (Z1 code analysis). The kinks along straight lines represent the polymer chain entanglements.

multiple disconnected paths is monotonically reduced, subject to chain-uncrossability. Upon iterating the geometrical procedure, each multiple disconnected path converges to a final state, the shortest disconnected path, i.e., an individual PP for each chain. The convergence of the Z1 code is achieved

once the difference between two successive iterations is smaller than a preset numerical tolerance. In short, the PP can be considered as the shortest path remaining when one holds chain ends fixed, while continuously reducing (shrinking) a chain's contours without violating topological constraints (polymer chain uncrossability).⁵⁷ A single PP is often characterized by its conformational properties such as PP length L_{pp} , number of interior kinks (or entanglements) Z , and the end-to-end distance R_{ee} . More details on the implementation and application of Z1 code in PP study of polymers can be found in refs 12–16, 56. In order to calculate the PP network of PE matrix, we consider two modes for the PP network analysis of PE nanocomposites. One is the so called “phantom particle limit”.²⁰ The nanoparticles in PNCs are ignored as we assume that the motion of the polymer chains is not constrained by these nanoparticles on the time scale of reptation dynamics. In that case, the nanoparticles are removed from the PNCs before the Z1 code^{15,16} is applied on the PE matrix to extract its corresponding PP network. In this situation, the effect of nanoparticles on the PP network can only appear as they may change the underlying topology of the PE matrix. In the other direction, the nanoparticles may behave as the “particle entanglements”, which behave as anchors to polymer chains and attach them together, then greatly restrict the motion of polymer chains. The other mode, i.e., “frozen particle limit” is also considered.²⁰ In the “frozen particle limit”, all the nanoparticles are fixed in the space, then the Z1 code is applied to extract the corresponding PP network. All the nanoparticles are treated in the same manner as the PE matrix, based on the same geometrical criteria. Basically, the nanoparticles surfaces are meshed by using artificial rodlike chains ($N = 2$ polymers), and we use the original Z1 code to find the shortest path. Since a dumbbell does not move (fixed ends), the chain length of such a single-segment rodlike chain is also irreducible. Within the analysis of the final shortest path, the nanoparticles have of course to be ignored, and they do not move during the minimization procedure. When the Z1 code is applied on PE nanocomposites with nanoparticles, we can calculate their corresponding PP network as shown in Figure 11. Since the size of the nanoparticles considered in the current work is comparable to the size of PE polymer chains, which can greatly restrict the dynamics of polymer chains, we only consider the “frozen particle limit” case for PP analysis.

B. Viscosity Calculation on PE Nanocomposites. The viscosities of pure PE and PE nanocomposites are obtained through NEMD simulations, based on the GSLLOD algorithm,⁵⁸ with appropriate boundary conditions for shear deformation, e.g., Lees–Edwards boundary conditions.⁵⁹ The GSLLOD algorithm⁵⁸ is derived from rigorous statistical-mechanics principles, and usually coupled with a Nose–Hoover thermostat^{60,61} for

simulations at constant temperature so that the canonical ensemble is generated with following form:⁵⁸

$$\begin{aligned}\dot{\mathbf{q}}_i &= \frac{\mathbf{p}_i}{m_i} + \mathbf{q}_i \cdot \nabla \mathbf{u}, \\ \dot{\mathbf{p}}_i &= \mathbf{F}_i - \mathbf{p}_i \cdot \nabla \mathbf{u} - m_i \mathbf{q}_i \cdot \nabla \mathbf{u} \cdot \nabla \mathbf{u} - \frac{p_\xi}{Q} \mathbf{p}_i, \\ \dot{\xi} &= \frac{p_\xi}{Q}, \\ \dot{p}_\xi &= \sum_{i=1}^N \frac{\mathbf{p}_i^2}{m_i} - dNk_B T\end{aligned}\quad (\text{A1})$$

In above equation, \mathbf{q}_i , \mathbf{p}_i , m_i , and \mathbf{F}_i are the position vector, momentum vector, mass, and force vector of each atom in molecule i , respectively, $d = 3$ is the space dimensionality, N is the total number of atoms in the system, ξ and p_ξ are the coordinate- and momentum-like variables, respectively, of the Nose–Hoover thermostat controlling the temperature of the system at desired level, $Q = dNk_B T\tau^2$ is the thermostat mass parameter. The relaxation time τ is set to be 0.4 ps in all simulations with a time step of 1 fs. In the NEMD approach, a shear velocity profile is applied to the system and the corresponding response via an off-diagonal component of the stress tensor is measured, which is proportional to the momentum flux. If we apply the Couette flow along the x -axis and the gradient of the flow is along the y -axis, the flow rate dependent shear viscosity can be obtained by

$$\eta = -\frac{\langle P_{xy} \rangle}{\dot{\gamma}} \quad (\text{A2})$$

where $\langle P_{xy} \rangle$ is the time average of xy - component of the pressure tensor and $\dot{\gamma}$ is the shear rate. In the current work, we had to limit our simulations to a very high strain rate, $10^9/\text{s}$. The motions of nanoparticles are frozen in the co-moving triclinic system (simulation box) to keep the distribution of nanoparticles and their orientations fixed. Thus, the nanoparticle centers are convected affinely with the shear flow, as shown in the inset of Figure 10. In the laboratory frame, these nanoparticles change distances all the time, and they behave as infinitely massed particles. The atom crossing a periodic boundary will have a delta added to its velocity equal to the difference in prescribed macroscopic velocities between the lower and higher boundaries. This velocity difference can include tilt components, e.g., a delta in the x velocity when an atom crosses the y periodic boundary, when the shear flow is applied along the x direction. Thus, such a boundary condition is equivalent to the Lees–Edwards boundary condition.⁵⁹ The total simulation time is about 10–20 ns to make sure that the system achieves the steady-state shear flow condition. The shear velocity v_x profile was also monitored by dividing the simulation box into 20 slabs along its y direction (Figure 10), when the flow is along the x -axis and the gradient of the flow is along the y -axis. A typical snapshot for the simulation box of PE/Bucky is also shown in the inset of Figure 10, with surrounding polymer chains made invisible. Under the high shear strain rates, the polymer chains in the simulation box tend to orient along with the shear flow. Therefore, in order to minimize finite system size effects, all the simulation cells have been increased three times along the flow direction. The side

lengths along the flow direction for PE, PE/Bucky, PE/Graphene, PE/ND, PE/Xjunction, and PE/Yjunction are 374.4, 368.5, 326.8, 402.6, 339.2, and 367.6 Å, respectively. The side lengths for other directions are 93.6, 92.1, 81.7, 100.7, 84.8, and 91.9 Å, respectively, for PE, PE/Bucky, PE/Graphene, PE/ND, PE/Xjunction, and PE/Yjunction. Fully equilibrated initial configurations (at all length scales) were used in the NEMD simulations. Since the orientational motions of nanoparticles are frozen, the obtained viscosities of PE nanocomposites are different along different directions, especially for PE/Graphene, PE/Xjunction, and PE/Yjunction. These anisotropic viscosities are only relevant for a system where these nanoparticles have a fixed orientation in space. This could be realized by magnetic nanoparticles in the presence of a strong external field. To this end, we are essentially studying the limit of strong magnetization by fixing the alignment of these nanoparticles, to explore their geometrical effects on the viscosity, which is typically done in the field of liquid crystals. The anisotropic viscosities are so called Miesowicz viscosities.⁶² In short, we study the effect of nanoparticle shape of perfectly aligned nanoparticles on the anisotropic viscosities within the necessarily non-Newtonian regime of the PE matrix, due to the limitation of computational power. These results allow us to get an impression about the maximum anisotropy one can expect to find in a system of oriented nanoparticles. The viscosity ultimately becomes isotropic but remains nanoparticle geometry-dependent if the nanoparticles are dispersed and convected non-affinely with the shear flow.

AUTHOR INFORMATION

Corresponding Author

*E-mail: w-liu@northwestern.edu (W.K.L.). Fax: 847-491-3915.

Notes

The authors declare no competing financial interest.

ACKNOWLEDGMENTS

We are grateful to the helpful discussions with Brendan Abberton, John Moore and Dr. Sinan Keten. This work is supported by NSF CMMI Grants 0823327, 0928320, and NSF IDR CMM Grant I 1130948. Y.L. acknowledges the partial financial support from Ryan Fellowship at Northwestern University. M.K. acknowledges support by SNSF grant IZ73Z0-128169. W.K.L. was also partially supported by the World Class University Program through the National Research Foundation of Korea (NRF) funded by the Ministry of Education, Science and Technology (R33-10079). This research used resources of the QUEST cluster at Northwestern University and the Argonne Leadership Computing Facility at Argonne National Laboratory, which is supported by the Office of Science of the U.S. Department of Energy under contract DE-AC02-06CH11357.

REFERENCES

- (1) Rouse, P. E. *J. Chem. Phys.* **1953**, *21*, 1272–1280.
- (2) de Gennes, P.-G. *J. Chem. Phys.* **1971**, *55*, 572.
- (3) Doi, M.; Edwards, S. F., *The theory of polymer dynamics*. Clarendon Press: Oxford, U.K., 1986.
- (4) Likhtman, A. E.; McLeish, T. C. B. *Macromolecules* **2002**, *35*, 6332–6343.
- (5) Wischnewski, A.; Monkenbusch, M.; Willner, L.; Richter, D.; Likhtman, A. E.; McLeish, T. C. B.; Farago, B. *Phys. Rev. Lett.* **2002**, *88*, 058301.
- (6) McLeish, T. C. B. *Adv. Phys.* **2002**, *51*, 1379–1527.
- (7) Bueche, F. *Reinforcement of elastomers*; Interscience Publishers: New York, 1965.
- (8) Schneider, G. J.; Nusser, K.; Willner, L.; Falus, P.; Richter, D. *Macromolecules* **2011**, *44*, 5857–5860.
- (9) Baig, C.; Mavrantzas, V. G.; Kröger, M. *Macromolecules* **2010**, *43*, 6886–6902.
- (10) Baig, C.; Stephanou, P. S.; Tsolou, G.; Mavrantzas, V. G.; Kröger, M. *Macromolecules* **2010**, *43*, 8239–8250.
- (11) Everaers, R.; Sukumaran, S. K.; Grest, G. S.; Svaneborg, C.; Sivasubramanian, A.; Kremer, K. *Science* **2004**, *303*, 823–826.
- (12) Foteinopoulou, K.; Karayiannis, N. C.; Laso, M.; Kröger, M. *J. Phys. Chem. B* **2009**, *113*, 442–455.
- (13) Hoy, R. S.; Foteinopoulou, K.; Kröger, M. *Phys Rev E* **2009**, *80*, 031803.
- (14) Karayiannis, N. C.; Kröger, M. *Int. J. Mol. Sci.* **2009**, *10*, 5054–5089.
- (15) Kröger, M. *Comput. Phys. Commun.* **2005**, *168*, 209–232.
- (16) Shanbhag, S.; Kröger, M. *Macromolecules* **2007**, *40*, 2897–2903.
- (17) Stephanou, P. S.; Baig, C.; Tsolou, G.; Mavrantzas, V. G.; Kröger, M. *J. Chem. Phys.* **2010**, *132*, 124904.
- (18) Tzoumanekas, C.; Theodorou, D. N. *Macromolecules* **2006**, *39*, 4592–4604.
- (19) Li, Y.; Kröger, M.; Liu, W. K. *Polymer* **2011**, *52*, 5867–5878.
- (20) Toepperwein, G. N.; Karayiannis, N. C.; Riggleman, R. A.; Kröger, M.; de Pablo, J. J. *J. Macromolecules* **2011**, *44*, 1034–1045.
- (21) Ramos, J.; Vega, J. F.; Theodorou, D. N.; Martinez-Salazar, J. *Macromolecules* **2008**, *41*, 2959–2962.
- (22) Riggleman, R. A.; Toepperwein, G.; Papakonstantopoulos, G. J.; Barrat, J. L.; de Pablo, J. J. *J. Chem. Phys.* **2009**, *130*, 244903.
- (23) Starr, F. W.; Douglas, J. F.; Glotzer, S. C. *J. Chem. Phys.* **2003**, *119*, 1777–1788.
- (24) Starr, F. W.; Knauert, S. T.; Douglas, J. F. *J. Polym. Sci., Polym. Phys.* **2007**, *45*, 1882–1897.
- (25) Starr, F. W.; Douglas, J. F. *Phys. Rev. Lett.* **2011**, *106*, 115702.
- (26) Ramanathan, T.; Abdala, A. A.; Stankovich, S.; Dikin, D. A.; Herrera-Alonso, M.; Pineri, R. D.; Adamson, D. H.; Schniepp, H. C.; Chen, X.; Ruoff, R. S.; Nguyen, S. T.; Aksay, I. A.; Prud'homme, R. K.; Brinson, L. C. *Nat. Nanotechnol.* **2008**, *3*, 327–331.
- (27) Potts, J. R.; Dreyer, D. R.; Bielawski, C. W.; Ruoff, R. S. *Polymer* **2011**, *52*, 5–25.
- (28) Li, Y.; Qiu, X. M.; Wang, M.; Yin, Y. J.; Yang, F.; Fan, Q. S. *EPL-Europhys Lett* **2009**, *88*, 26006.
- (29) Li, Y.; Qiu, X. M.; Yang, F.; Yin, Y. J.; Fan, Q. S. *Carbon* **2009**, *47*, 812–819.
- (30) Zsoldos, I.; Kakuk, G.; Reti, T.; Szasz, A. *Model. Simulat. Mater. Sci. Eng.* **2004**, *12*, 1251–1266.
- (31) <http://accelrys.com/products/materials-studio/>
- (32) Flory, P. J. *Statistical Mechanics of Chain Molecules*. Oxford University Press: New York, 1988.
- (33) Mondello, M.; Grest, G. S.; Webb, E. B.; Peczak, P. *J. Chem. Phys.* **1998**, *109*, 798–805.
- (34) Adnan, A.; Sun, C. T.; Mahfuz, H. *Compos. Sci. Technol.* **2007**, *67*, 348–356.
- (35) Hossain, D.; Tschoopp, M. A.; Ward, D. K.; Bouvard, J. L.; Wang, P.; Horstemeyer, M. F. *Polymer* **2010**, *51*, 6071–6083.
- (36) Capaldi, F. M.; Boyce, M. C.; Rutledge, G. C. *Polymer* **2004**, *45*, 1391–1399.
- (37) Chen, I. W. P.; Liang, Z. Y.; Wang, B.; Zhang, C. *Carbon* **2010**, *48*, 1064–1069.
- (38) Li, Y. *Polymer* **2011**, *52*, 2310–2318.
- (39) Sun, X. Q.; Lin, T.; Gezelter, J. D. *J. Chem. Phys.* **2008**, *128*.
- (40) Plimpton, S. *J. Comput. Phys.* **1995**, *117*, 1–19.
- (41) Kröger, M.; Hess, S. *Phys. Rev. Lett.* **2000**, *85*, 1128–1131.
- (42) Lebovitz, A. H.; Khait, K.; Torkelson, J. M. *Macromolecules* **2002**, *35*, 8672–8675.
- (43) Kröger, M.; Ilg, P. *J. Chem. Phys.* **2007**, *127*, 034903.
- (44) Stockelhuber, K. W.; Svistkov, A. S.; Pelevin, A. G.; Heinrich, G. *Macromolecules* **2011**, *44*, 4366–4381.

- (45) Starr, F. W.; Schroder, T. B.; Glotzer, S. C. *Macromolecules* **2002**, *35*, 4481–4492.
- (46) Ndoro, T. V. M.; Voyatzis, E.; Ghanbari, A.; Theodorou, D. N.; Bohm, M. C.; Muller-Plathe, F. *Macromolecules* **2011**, *44*, 2316–2327.
- (47) Raos, G.; Moreno, M.; Elli, S. *Macromolecules* **2006**, *39*, 6744–6751.
- (48) Papakonstantopoulos, G. J.; Doxastakis, M.; Nealey, P. F.; Barrat, J. L.; de Pablo, J. J. *Phys. Rev. E* **2007**, *75*, 031803.
- (49) Fetters, L. J.; Lohse, D. J.; Richter, D.; Witten, T. A.; Zirkel, A. *Macromolecules* **1994**, *27*, 4639–4647.
- (50) Okuda, S.; Inoue, Y.; Masubuchi, Y.; Uneyama, T.; Hojo, M. *J. Chem. Phys.* **2009**, *130*, 214907.
- (51) Papon, A.; Saalwachter, K.; Schaler, K.; Guy, L.; Lequeux, F.; Montes, H. *Macromolecules* **2011**, *44*, 913–922.
- (52) Pearson, D. S.; Strate, G. V.; Vonmeerwall, E.; Schilling, F. C. *Macromolecules* **1987**, *20*, 1133–1141.
- (53) Knauer, S. T.; Douglas, J. F.; Starr, F. W. *J. Polym. Sci., Polym. Phys.* **2007**, *45*, 1882–1897.
- (54) Heine, D. R.; Petersen, M. K.; Grest, G. S. *J. Chem. Phys.* **2010**, *132*, 184509.
- (55) Petersen, M. K.; Lane, J. M. D.; Grest, G. S. *Phys. Rev. E* **2010**, *82*, 010201(R).
- (56) Foteinopoulou, K.; Karayannidis, N. C.; Mavrantzas, V. G.; Kröger, M. *Macromolecules* **2006**, *39*, 4207–4216.
- (57) Tzoumanekas, C.; Theodorou, D. N. *Curr. Opin. Solid State Mater. Sci.* **2006**, *10*, 61–72.
- (58) Tuckerman, M. E.; Mundy, C. J.; Balasubramanian, S.; Klein, M. L. *J. Chem. Phys.* **1997**, *106*, 5615–5621.
- (59) Lees, A. W.; Edwards, S. F. *J. Phys., Part C Solid* **1972**, *5*, 1921–1929.
- (60) Nose, S. *Mol. Phys.* **1984**, *52*, 255–268.
- (61) Hoover, W. G. *Phys. Rev. A* **1985**, *31*, 1695–1697.
- (62) Kröger, M.; Sellers, H. S. *J. Chem. Phys.* **1995**, *103*, 807–817.